Focusing light into deep subwavelength using metamaterial immersion lenses

Changbao Ma and Zhaowei Liu*

Department of Electrical and Computer Engineering, University of California, San Diego, 9500 Gilman Drive, La Jolla, CA 92093-0407, USA
**zhaowei@ece.ucsd.edu*

Abstract: We propose and demonstrate metamaterial immersion lenses by shaping plasmonic metamaterials. The convex and concave shapes for the elliptically and hyperbolically dispersive metamaterials are designed using phase compensation method. Numerical simulations verify that the metamaterial immersion lenses possess exceptionally large effective numerical apertures thus can achieve deep subwavelength resolution focusing. We also discuss the importance of the losses in modulating the optical transfer function and thus in enhancing the performance of the metamaterial immersion lenses.

© 2010 Optical Society of America

OCIS codes: (160.3918) Metamaterials; (220.3630) Lenses; (350.5730) Resolution; (350.4238) Nanophotonics.

References and links

1. E. Abbe, "Beitrage zur Theorie des Mikroskops und der mikroskopischen Wahrnehmung," Arch. Mikroskop. Anat. **9**(1), 413–418 (1873).
2. X. Zhang, and Z. Liu, "Superlenses to overcome the diffraction limit," Nat. Mater. **7**(6), 435–441 (2008).
3. N. Fang, H. Lee, C. Sun, and X. Zhang, "Sub-diffraction-limited optical imaging with a silver superlens," Science **308**(5721), 534–537 (2005).
4. Z. Liu, S. Durant, H. Lee, Y. Pikus, N. Fang, Y. Xiong, C. Sun, and X. Zhang, "Far-field optical superlens," Nano Lett. **7**(2), 403–408 (2007).
5. E. E. Narimanov, "Far-field superlens: Optical Nanoscope," Nat. Photonics **1**(5), 260–261 (2007).
6. Z. Jacob, L. V. Alekseyev, and E. Narimanov, "Optical Hyperlens: Far-field imaging beyond the diffraction limit," Opt. Express **14**(18), 8247–8256 (2006).
7. Z. Liu, H. Lee, Y. Xiong, C. Sun, and X. Zhang, "Far-field optical hyperlens magnifying sub-diffraction-limited objects," Science **315**(5819), 1686 (2007).
8. Y. Xiong, Z. Liu, and X. Zhang, "A simple design of flat hyperlens for lithography and imaging with half-pitch resolution down to 20 nm," Appl. Phys. Lett. **94**(20), 203108 (2009).
9. I. I. Smolyaninov, Y. J. Hung, and C. C. Davis, "Magnifying superlens in the visible frequency range," Science **315**(5819), 1699–1701 (2007).
10. S. Vedantam, H. Lee, J. Tang, J. Conway, M. Staffaroni, and E. Yablonovitch, "A Plasmonic Dimple Lens for Nanoscale Focusing of Light," Nano Lett. **9**(10), 3447–3452 (2009).
11. F. M. Huang, and N. I. Zheludev, "Super-resolution without evanescent waves," Nano Lett. **9**(3), 1249–1254 (2009).
12. L. Verslegers, P. B. Catrysse, Z. Yu, and S. Fan, "Deep-Subwavelength Focusing and Steering of Light in an Aperiodic Metallic Waveguide Array," Appl. Phys. Lett. **103**(3), 033902–033904 (2009).
13. S. M. Mansfield, and G. S. Kino, "Solid immersion microscope," Appl. Phys. Lett. **57**(24), 2615–2616 (1990).
14. L. P. Ghislain, and V. B. Elings, "Near-field scanning solid immersion microscope," Appl. Phys. Lett. **72**(22), 2779–2781 (1998).
15. L. P. Ghislain, V. B. Elings, K. B. Crozier, S. R. Manalis, S. C. Minne, K. Wilder, G. S. Kino, and C. F. Quate, "Near-field photolithography with a solid immersion lens," Appl. Phys. Lett. **74**(4), 501–503 (1999).
16. M. Rothschild, T. M. Bloomstein, R. R. Kunz, V. Liberman, M. Switkes, S. T. Palmacci, J. H. C. Sedlacek, D. Hardy, and A. Grenville, "Liquid immersion lithography: Why, how, and when?" J. Vac. Sci. Technol. B **22**(6), 2877–2881 (2004).
17. B. D. Terris, H. J. Mamin, D. Rugar, W. R. Studenmund, and G. S. Kino, "Near-field optical data storage using a solid immersion lens," Appl. Phys. Lett. **65**(4), 388–390 (1994).
18. H. F. Hamann, Y. C. Martin, and H. K. Wickramasinghe, "Thermally assisted recording beyond traditional limits," Appl. Phys. Lett. **84**(5), 810–812 (2004).

#123382 - $15.00 USD Received 27 Jan 2010; revised 11 Feb 2010; accepted 12 Feb 2010; published 23 Feb 2010
(C) 2010 OSA

19. Q. Wu, G. D. Feke, R. D. Grober, and L. P. Ghislain, "Realization of numerical aperture 2.0 using a gallium phosphide solid immersion lens," Appl. Phys. Lett. **75**(26), 4064–4066 (1999).
20. S. B. Ippolito, B. B. Goldberg, and M. S. Unlu, "High spatial resolution subsurface microscopy," Appl. Phys. Lett. **78**(26), 4071–4073 (2001).
21. D. R. Smith, J. B. Pendry, and M. C. K. Wiltshire, "Metamaterials and negative refractive index," Science **305**(5685), 788–792 (2004).
22. V. Shalaev, "Optical negative-index metamaterials," Nat. Photonics **1**(1), 41–48 (2007).
23. J. Yao, Z. Liu, Y. Liu, Y. Wang, C. Sun, G. Bartal, A. M. Stacy, and X. Zhang, "Optical negative refraction in bulk metamaterials of nanowires," Science **321**(5891), 930 (2008).
24. G. Kino, "The solid immersion lens," Proc. SPIE **3740**, 2–6 (1999).
25. S. A. Ramakrishna, J. B. Pendry, M. C. K. Wiltshire, and W. J. Stewart, "Imaging the near field," J. Mod. Opt. **50**, 1419–1430 (2003).
26. K. Iizuka, *Elements of Photonics vol. 1* (John Wiley & Sons, New York, 2002).
27. J. Pendry, A. Holden, D. Robbins, and W. Stewart, "Low frequency plasmons in thin-wire structures," J.Phys.-Condens. Matter **10**(22), 4785–4809 (1998).
28. J. Yao, Z. Liu, Y. Liu, Y. Wang, C. Sun, G. Bartal, A. M. Stacy, and X. Zhang, "Optical Negative Refraction in Bulk Metamaterials of Nanowires," Science **321**(5891), 930 (2008).
29. W. Srituravanich, L. Pan, Y. Wang, C. Sun, D. B. Bogy, and X. Zhang, "Flying plasmonic lens in the near field for high-speed nanolithography," Nat. Nanotechnol. **3**(12), 733–737 (2008).
30. H. I. Smith, R. Menon, A. Patel, D. Chao, M. Walsh, and G. Barbastathis, "Zone-plate-array lithography: A low-cost complement or competitor to scanning-electron-beam lithography," Microelectron. Eng. **83**(4-9), 956–961 (2006).
31. R. Völkel, H. P. Herzig, P. Nussbaum, R. Dandliker, and W. B. Hugle, "Microlens array imaging system for photolithography," Opt. Eng. **35**(11), 3323–3330 (1996).

1. Introduction

The transverse spatial resolution of conventional optical lenses is limited by the diffraction nature of the light to $\lambda/(2NA)$, with λ being the wavelength of light and NA being the numerical aperture of the lens [1]. Although various remarkable methods [2], including superlens [3–5], hyperlens [6–9], plasmonic dimple lens [10], super oscillation [11], aperiodic metallic waveguide array [12], etc. have been proposed to achieve resolution beyond the diffraction limit, the immersion technique is still widely used in oil immersion microscopy, solid immersion microscopy [13], near-field scanning solid immersion microscopy [14], photolithography [15,16], near-field optical data storage [17], heat/thermally assisted magnetic recording [18], etc. for resolution improvement due to its simplicity. Because the NA of an immersion lens is increased by a factor of the refractive index n, the corresponding resolution also improves n times. Many efforts have been taken to increase the NA by introducing various high index materials. Wu et al. reported an NA of 2.0 using a Gallium Phosphide solid immersion lens (SIL) in the visible band [19]. Using the NA increasing lens (NAIL) technique, an NA as high as 3.3 was achieved with Silicon in the infrared band by Ippolito et al [20]. However, the resolution improvement by immersion techniques remains modest due to the lack of high-index transparent materials. Metamaterials [21–23], which are artificially engineered composites of nanoscale metallic/dielectric structures, have demonstrated their ability to achieve extraordinary phenomena and devices, due to their exceptional electromagnetic properties that are not achievable in natural materials. In this article, we propose for the first time a new type of immersion lens based on metamaterials, i.e., metamaterial immersion lens (MIL). The MILs can achieve super resolution and can be easily integrated with conventional optical systems.

2. Theory

It is commonly known that only the light from a point source within a small cone inside a high-index flat slab can transmit to air. The light outside that light cone will be totally reflected. For this reason, the shape of an SIL is not a flat but a curved high-index slab, such as a hemisphere or a supersphere [24]. Therefore, all the high k-vector waves supported by the SIL can be coupled into the lens from free space. Moreover, the phases of the incident waves are well compensated by the appropriate shape of the SIL, leading to constructive and high resolution focusing. A metamaterial slab may be easily designed to cover high k-vectors, so

#123382 - $15.00 USD Received 27 Jan 2010; revised 11 Feb 2010; accepted 12 Feb 2010; published 23 Feb 2010
(C) 2010 OSA

the small light cone phenomenon maintains similarly as in the high-index isotropic slab discussed above. In analogy to an isotropic high-index SIL, we shape the interface of a metamaterial to achieve the bidirectional coupling between the metamaterial and air with well designed phase compensation. By replacing the isotropic transparent dielectrics with metamaterial, the MIL possesses unprecedented resolving power when compared with conventional SIL.

The idea may be illustrated with a two-dimensional (2D) highly anisotropic metamaterial, which may have either elliptic ($\varepsilon_x' > 0$, $\varepsilon_z' > 0$) or hyperbolic ($\varepsilon_x' > 0$, $\varepsilon_z' < 0$) dispersion. Here ε_x' and ε_z' are the real part of the permittivity of the metamaterial in the x and z directions, respectively. The wavefront of a line light source inside such a metamaterial slab may be either convex for elliptic dispersion or concave for hyperbolic dispersion. Accordingly, a metamaterial may be shaped to have either a convex surface for elliptic dispersion or a concave surface for hyperbolic dispersion to achieve the coupling and phase compensation, due to the similarity between the interface shape and the dispersion curve of the metamaterial. Figure 1 shows the dispersion curves (Equifrenquency curves, EFCs) of air and the metamaterials. Let us assume that the principle axes of the metamaterials are always along the horizontal (k_x) and vertical (k_z) directions. When the interface of the metamaterial is along the k_x axis, only the incident light within a small light cone with the transverse k-vectors less than k_0 can transmit into and out of the metamaterial, as shown in Fig. 1(a). Figures 1(b) and 1(c) show that the transverse k-vector coverage can be enlarged from k_0 to k_1 when the interface of the metamaterial (k_{xt} axis) has an angle with respect to the material principle axes. Each point on the curved interface of the metamaterial may be considered having an interface not in the x axis direction, thus the transverse k-vector coverage can be extended by a curved interface. As shown in Figs. 1(b) and 1(c), the extended wavevector coverage k_1 can be much larger than k_0 and even the highest achievable k-vectors in natural SIL materials, so super resolution can be achieved. In the following, we demonstrate the MIL concept with both elliptic (referred to as an elliptic MIL) and hyperbolic (referred to as a hyperbolic MIL) dispersions based on phase compensation for focusing in the metamaterials and numerically verify the analysis and designs.

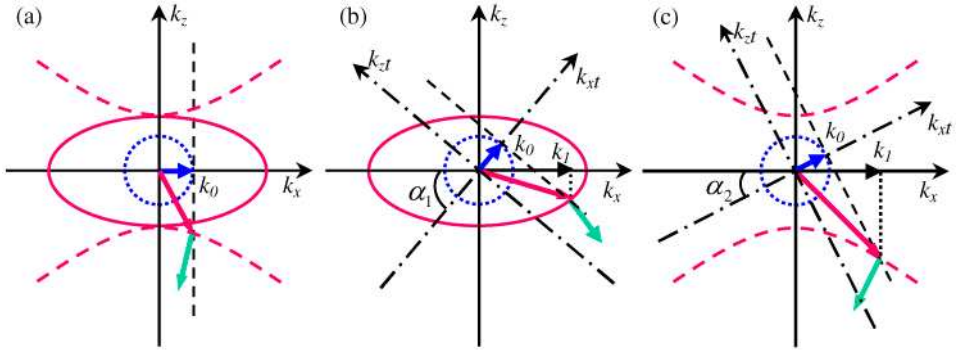

Fig. 1. Equifrequency curves (EFCs) of air (dotted blue circle) and the metamaterials with an elliptic (solid red ellipse) and a hyperbolic (dashed red hyperbola) dispersion, respectively. (a) The interface of the metamaterials is a straight line along the k_x direction; (b) The interface of the metamaterial with an elliptic dispersion has an angle α_1 with respect to the k_x axis; (c) The interface of the metamaterial with an hyperbolic dispersion has an angle α_2 with respect to the k_x axis. That is, the k_{xt} axis is the interface in both (b) and (c).

3. Formulations and simulations

Figure 2(a) shows the schematic of an elliptic MIL. Assuming designing an elliptic MIL with a focal length of f_m and $x \in [-x_{\max}, x_{\max}]$. When a plane wave is incident on the MIL from the

#123382 - $15.00 USD Received 27 Jan 2010; revised 11 Feb 2010; accepted 12 Feb 2010; published 23 Feb 2010
(C) 2010 OSA

top, then refracted by the interface curve and focused to F_m. Phase condition for constructive interference at F_m results in the following quadratic equation

$$k_0(h_0 n + \sqrt{\varepsilon_x' f_m^2 + \varepsilon_z' x_{\max}^2}) = k_0[(h_0 - h)n + \sqrt{\varepsilon_x'(f_m + h)^2 + \varepsilon_z' x^2}] \quad (1)$$

Therefore,

$$h(x) = (-b + \sqrt{b^2 - 4ac})/(2a) \quad (2)$$

where $a = \varepsilon_x' - n^2$, $b = 2f_m\varepsilon_x' - 2n\sqrt{\varepsilon_x' f_m^2 + \varepsilon_z' x_{\max}^2}$, $c = \varepsilon_z'(x^2 - x_{\max}^2)$ and k_0 being the wavevector in free space. Note that the other solution of Eq. (1) makes the position of F_m outside the metamaterial, and thus not suitable for MIL purpose. With Eq. (2), the interface shape of the elliptic MIL can be calculated. Equations (1) and (2) are derived for an elliptic MIL. Changing ε_z' to be negative results in the formulas for the hyperbolic MIL, with $x_{\max} < f_m \tan\beta$ and $\tan\beta = \sqrt{-\varepsilon_x'/\varepsilon_z'}$. The sign change of ε_z' for the hyperbolic MIL case can be easily verified using the schematic of the hyperbolic MIL in Fig. 2(b). If measured from the apex of the curved interfaces, then the focal lengths are $f = (f_m + h_0)$, with h_0 is positive for the elliptic MIL and negative for the hyperbolic MIL.

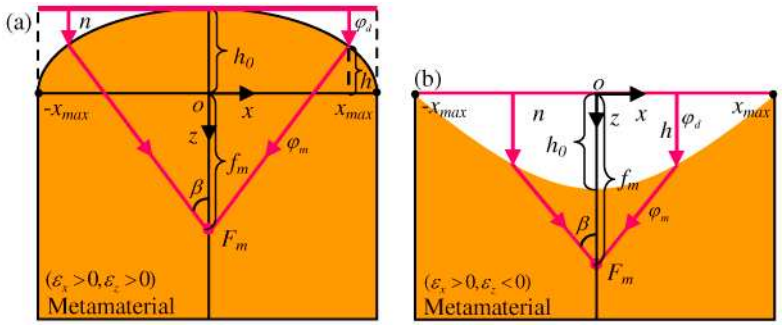

Fig. 2. Schematics of (a) an elliptic and (b) a hyperbolic metamaterial immersion lens.

Simulations have been carried out to verify the analysis above for both cases at the wavelength of 633 nm. Figure 3(a) shows the simulated power profile of an elliptic MIL with a normal incidence of plane wave. The permittivity of the elliptic metamaterial is ε_x = 5.1 + 0.1i and ε_z = 16.0 + 0.08i, which is designed using an alternate multilayer [25] of silver and Gallium Phosphide [19] with a volume filing factor of silver to the metamaterial of p = 0.2.

#123382 - $15.00 USD Received 27 Jan 2010; revised 11 Feb 2010; accepted 12 Feb 2010; published 23 Feb 2010
(C) 2010 OSA

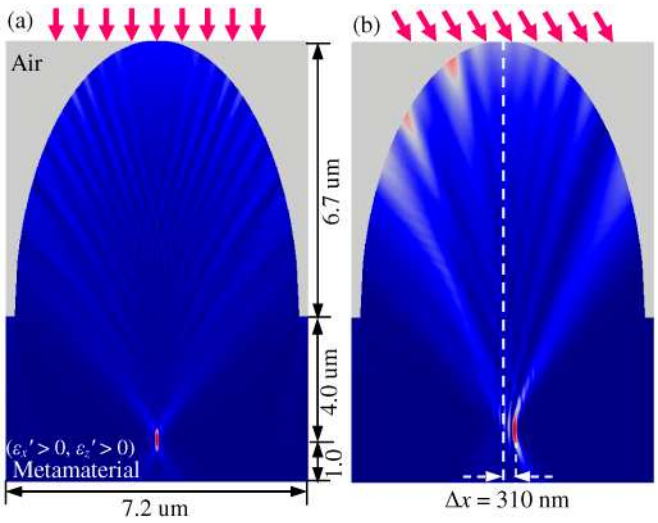

Fig. 3. Simulations of an elliptic MIL with (a) normal and (b) oblique incidence of plane wave.

The multiple layers of the metamaterial lay in the x direction in the MIL. The focal length of the elliptic MIL is f_m = 3 um and x_{max} = 3.4 um, and the calculated h_0 = 6.7 um. This elliptic MIL achieved a focus with an FWHM (full width at half maximum) of 70 nm (~λ/9) for the normal plane wave incidence, which is equivalent to an effective NA of 4.5.

When the incident light is tilted, the focus will be shifted accordingly. The shift may be estimated by using [26]

$$\Delta x = \mathrm{Re}(f\sqrt{\varepsilon_x / \varepsilon_z} / \sqrt{\varepsilon_z - \sin^2\theta}\sin\theta) \tag{3}$$

where θ is the incident angle with respect to the z axis and Re denotes the real part. In practical designing, $|\varepsilon_z'| >> \sin^2\theta$, so Eq. (3) can be reduced to

$$\Delta x \approx \mathrm{Re}(f\sqrt{\varepsilon_x} / \varepsilon_z \sin\theta) \tag{4}$$

The simulation in Fig. 3(b) shows a shift of Δx = 310 nm for θ = 14 degrees, which is comparable to the calculated shift Δx = 331 nm.

The elliptic MIL above has shown its unprecedented high resolution performance over conventional homogeneous SILs, due to its high optical anisotropy. The hyperbolic MIL may behaves differently due to the negative ε_z'. Figure 4(a) shows the simulated power profile of a hyperbolic MIL with a normal incidence of plane wave. The permittivity of the elliptic metamaterial is ε_x = 8.1 + 0.1i and ε_z = −12.5 + 0.3i, which is designed using silver nanowires [27] in air background with a silver volume filing factor of p = 0.7. The silver nanowires of the metamaterial are aligned in the z direction. The focal length of the elliptic MIL is f_m = 2 um and x_{max} = 1.29 um, and the calculated h_0 = −1.23 um. This hyperbolic MIL achieved a focus with an FWHM of 66 nm (~λ/9.6) for the normal plane wave incidence, which is equivalent to an effective NA of 4.8. As in the elliptic MIL, when the incident light is tilted, the focus will be shifted. The simulation in Fig. 4(b) shows a shift of Δx = −120 nm for θ = 37.8 degrees to the opposite side to the elliptic MIL. This shift is also comparable to the calculated shift Δx = −108 nm using Eq. (3).

#123382 - $15.00 USD Received 27 Jan 2010; revised 11 Feb 2010; accepted 12 Feb 2010; published 23 Feb 2010
(C) 2010 OSA

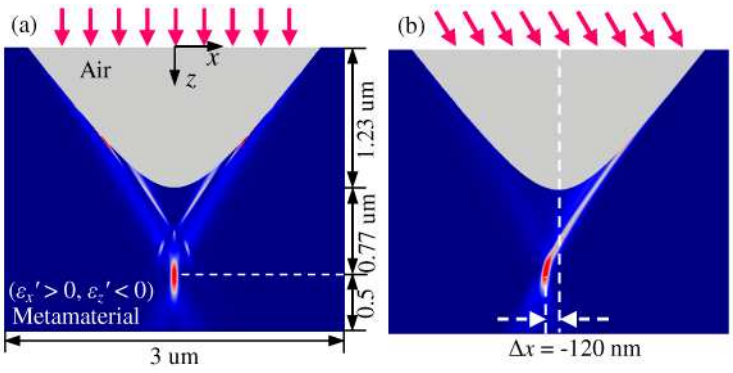

Fig. 4. Simulations of a hyperbolic MIL with (a) normal and (b) oblique incidence of plane wave.

4. Discussions and conclusions

As is demonstrated above, the elliptic and hyperbolic MILs can achieve super resolution with convex and concave interfaces, respectively. It is worth emphasizing that the hyperbolic MIL achieves focusing by a concave interface, which is exceptional and not achievable in conventional optics. With the designed curved interfaces, waves with high transverse *k*-vectors can be coupled into the metamaterial with compensated phase and thus can be focused into deep subwavelength scale. Notice that the concave interface of the hyperbolic MIL in Fig. 4 is flatter than that of the elliptic MIL in Fig. 3. This is due to the higher anisotropy, i.e., $|\varepsilon_z'|/\varepsilon_x'$, of the elliptic MIL than the hyperbolic MIL. While both types of MIL can achieve super resolution, the hyperbolic MIL shows anomalous imaging behavior. The opposite displacement of the focus with respect to the incident light is drastically different from the case that as normally been observed in conventional optical lenses. The new phenomenon originates from the negative refraction experienced at the metamaterial/air interface [28] that may open up new possibilities to design lens system with extraordinary functionalities and performances.

There are two major factors affecting the achievable resolution of the MILs: (i) the intrinsic material properties of the metamaterial. i.e. the *k*-vector coverage determined by the dispersion relation $k_z^2/\varepsilon_x + k_x^2/\varepsilon_z = k_0^2$ of the metamaterials, and (ii) the losses, including propagation and coupling losses, which may strongly modulate the optical transfer function (OTF) of the MILs. The dispersion relation imposes a theoretical cutoff on the coverage of k_x, which limits k_x up to $\mathrm{Re}(\sqrt{\varepsilon_z}k_0)$, for an elliptically dispersive metamaterial. On the other hand, the k_x has no limit in the dispersion relation of a hyperbolically dispersive metamaterial. The losses also play an important role in the performance of the MILs. Different *k*-vectors may have different loss coefficients and propagation lengths in an MIL, thus the *k*-vectors attenuate differently. Furthermore, the curved shapes of the MILs cause different refraction (coupling) efficiencies at different positions due to the different angles of incidence. The *k*-vector spectrum at the focus of an MIL may be significantly modulated by both the propagation and coupling losses and thus substantially different from that of a conventional SIL. The presented elliptic MIL achieved an effective NA of 4.5, which is even a little larger than $\mathrm{Re}(\sqrt{\varepsilon_z})$, i.e., 4.0. As shown in Fig. 3, the low transverse *k*-vectors in the center part propagate longer distances to the focus than the high *k*-vectors on the edge parts, so the low *k*-vectors attenuates more than the high *k*-vectors. Although the coupling efficiencies of at the center part in Fig. 3 are higher than on the edge parts for normal incidence, the coupling loss profile that makes the OTF is overwhelmed by the propagation losses. Therefore, the overall OTF of the elliptical MIL indicates more transmission for higher *k*-vector waves to the focus,

#123382 - $15.00 USD Received 27 Jan 2010; revised 11 Feb 2010; accepted 12 Feb 2010; published 23 Feb 2010
(C) 2010 OSA

i.e., more high k-vector contributions to the focus than in the case of a conventional lens, finally resulting in a higher resolution focus and a higher effective NA. In principle, k_x's of a hyperbolic MIL can be infinitely large as there is no cutoff in its dispersion relation, so extremely large effective NA's may be obtained. However, in practice, the chosen x_{max} limits the coverage of k_x. In the presented hyperbolic MIL above, the maximum k_x is $4.72k_0$. The loss mechanisms affect the performance of the hyperbolic MIL similarly as in the elliptic MIL, resulting in a higher NA of 4.8.

The metamaterials properties used in the examples above are real values based on the effective media estimation in 2D metal/dielectric multilayer composites [25] and metallic nanowires [27] in dielectric template at the visible wavelength of 633 nm. Because the metals are highly dispersive, non-monochromatic illumination may reduce the focusing performance of the MILs. Nonetheless, an MIL for a particular band of frequencies can always be optimized by taking the material dispersion into account. The elliptic and hyperbolic MIL concepts can be easily extended to three-dimensional (3D) devices and other frequency bands, such as ultraviolet, infrared, terahertz, or microwave. The same principle can also be applied to acoustics due to the nature of waves. The presented MILs have achieved super resolution and NAs. The ultimate limitation of MILs is not limited by these examples and can be designed to achieve much higher NAs. A practical usage of the MIL is to make its bottom plane the focal plane so that the resulting near field can be used [12]. As a result, the MIL can find extraordinary applications in lithography, imaging, scanning near-field microscope, sensing, optical storage and heat assisted magnetic recording, etc. As the MILs are typically in microscale, MILs can also be integrated with a flying head for high speed processing as in the flying plasmonic lens [29], and even an array of MILs can be designed for parallel processing [30,31].

#123382 - $15.00 USD Received 27 Jan 2010; revised 11 Feb 2010; accepted 12 Feb 2010; published 23 Feb 2010
(C) 2010 OSA